Surface & Coatings Technology 309 (2017) 490–496

Contents lists available at ScienceDirect

Surface & Coatings Technology

journal homepage: www.elsevier.com/locate/surfcoat

Effects of one-step hydrothermal treatment on the surface morphology and corrosion resistance of ZK60 magnesium alloy

Ruizhen Xu [a,b], Yi Shen [a], Jiangshan Zheng [a], Qiang Wen [a], Zhi Li [a], Xiongbo Yang [a,*], Paul K. Chu [b,*]

[a] College of Science, China Three Gorges University, Yichang 443002, China
[b] Department of Physics and Materials Science, City University of Hong Kong, Tat Chee Avenue, Kowloon, Hong Kong, China

ARTICLE INFO

Article history:
Received 4 October 2016
Revised 26 November 2016
Accepted in revised form 30 November 2016
Available online 02 December 2016

Keywords:
Magnesium alloy
Hydrothermal treatment
Corrosion resistance

ABSTRACT

A one-step hydrothermal method is employed to produce protective magnesium hydroxide films on ZK60 magnesium alloy samples. Samples with morphologies resembling small flakes, strips, and hexagonal flakes are produced depending on the preparation temperature and time. A higher temperature accelerates nucleation and growth of $Mg(OH)_2$ and the morphology of $Mg(OH)_2$ depends on the treatment time. The sample prepared at 120 °C for 24 h is covered by a 1.78 μm thick magnesium hydroxide film with the preferred (101) orientation and exhibits the best corrosion resistance. The results disclose a simple and environmental friendly method to protect the magnesium alloy by forming a self-sacrificing layer of $Mg(OH)_2$.

1. Introduction

Bone replacements are required to treat orthopedic diseases, injuries, and aging [1,2] and there are nearly 9 million annual fractures [3]. Commercial implants made of ceramics, metals, or polymers have some clinical limitations such as unsatisfactory mechanical properties and biocompatibility. Biodegradable materials have recently attracted considerable interests because they offer the necessary mechanical support before natural degradation inside the body thus obviating the need for a second surgery after healing. Owing to the excellent mechanical properties, biodegradability, and biocompatibility, magnesium and its alloys have been studied as potential biomaterials [4,5]. However, application of magnesium alloys have been plagued by the fast corrosion rate especially in the physiological environment [6]. To improve the corrosion resistance of magnesium alloys, some techniques such as chemical conversion [7,8], alloying [9], plasma immersion ion implantation and deposition (PIII&D) [10,11], electrochemical method [12], and coating deposition [13] have been studied. Among them, the hydrothermal (HT) method [14–16] is quite attractive due to the simple one-step process, environmental friendliness, and easy design of the reaction conditions.

The corrosion properties of magnesium alloys can be enhanced by the formation of oxide and/or hydroxide films [15]. MgO and $Mg(OH)_2$ constitute good protective films on account of the nontoxic and biocompatible properties. Zhang et al. and Ou et al. synthesized microstructured oxide or hydroxide layers by HT using water [17,18]. In addition, Ishizaki et al. coated $Mg(OH)_2$ on AZ31 by HT in an aqueous ammonium solution at different temperature [19], Zhu et al. synthesized magnesium hydroxide on AZ31 by HT in a NaOH solution as well as deionized water [15,20,21], and Feng et al. studied $Mg(OH)_2$ films prepared on AZ91 by HT at different pH for different time [21]. The *in situ* hydrothermal method was used to produce uniform $Mg(OH)_2$ films with good adhesion strength and protection of the substrate [22].

In this work, ZK60 magnesium alloy samples are treated by the alkaline HT method at different temperature and for various time durations. The films are characterized by field-emission scanning electron microscopy (FE-SEM), energy-dispersive X-ray spectroscopy (EDS), and X-ray diffraction (XRD) and the corrosion behavior is evaluated by potentiodynamic polarization tests.

2. Materials and methods

The ZK60 (Mg - 5.19 wt% Zn - 0.53 wt% Zr) specimens with dimensions of 10 mm × 10 mm × 5 mm were ground successively with up to 1200 grit *SiC* abrasive paper, ultrasonically rinsed with ethanol, and dried in air. The $Mg(OH)_2$ films were synthesized in a 1 M Na_2CO_3 solution. The solution was poured into a hydrothermal reaction vessel made of Teflon-lined stainless steel to fill 75% of the total volume. The raw ZK60 samples were put into the vessel and heated to different temperature of 60 and 120 °C in an electric oven and kept in the container for 1, 8, and 24 h, respectively.

Field-emission scanning electron microscopy (FE-SEM, JEOL JSM-7500F) and energy-dispersive X-ray spectroscopy (EDS) were performed to characterize the morphology and cross sections of the films. The elemental composition and chemical states were determined by X-ray photoelectron spectroscopy (XPS, Physical Electronics PHI 5802). The structure and orientation of the films were determined by X-ray diffraction (XRD) on an Ultima IV-3 kW XRD using CuK_α radiation

* Corresponding authors.
E-mail addresses: shiheren@hotmail.com (X. Yang), paul.chu@cityu.edu.hk (P.K. Chu).

http://dx.doi.org/10.1016/j.surfcoat.2016.11.111
0257-8972/

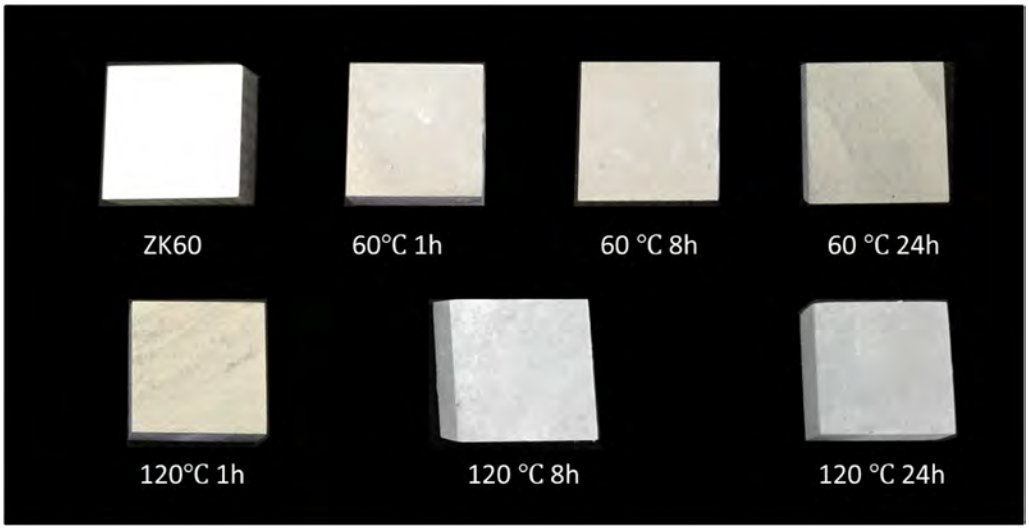

Fig. 1. Optical pictures revealing the surface morphologies of the ZK60 samples before and after hydrothermal treatment at different temperature and for different time.

($\lambda = 0.154$ nm). The analysis was conducted at 40 kV and 40 mA in the 2θ range of 20-80° at a step interval of 0.02. The corrosion properties were determined on a CHI660D electrochemical workstation based on a three electrode cell in which the sample, platinum rod, and saturated calomel electrode (SCE) served as the working, counter and reference electrodes, respectively. An area of 10 mm × 10 mm was exposed to the phosphate buffered saline (PBS, Boster Biological Technology Co. Ltd., Wuhan, China) solution at room temperature. PBS is a buffer

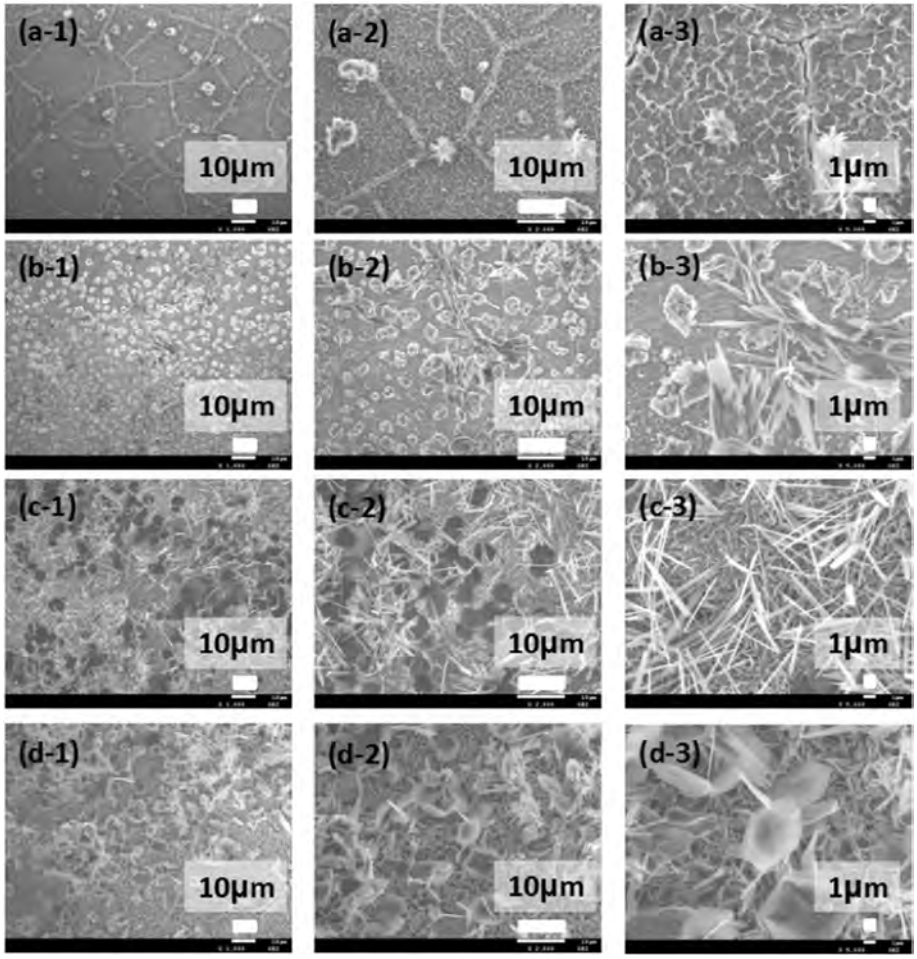

Fig. 2. Surface morphology of the ZK60 samples revealed by FE-SEM after the hydrothermal treatment: (a) 60 °C 24 h, (b)120 °C 1 h, (c) 120 °C 8 h, and (d)120 °C 24 h. The magnifications in (1), (2), (3) are 1000, 2000, and 5000, respectively.

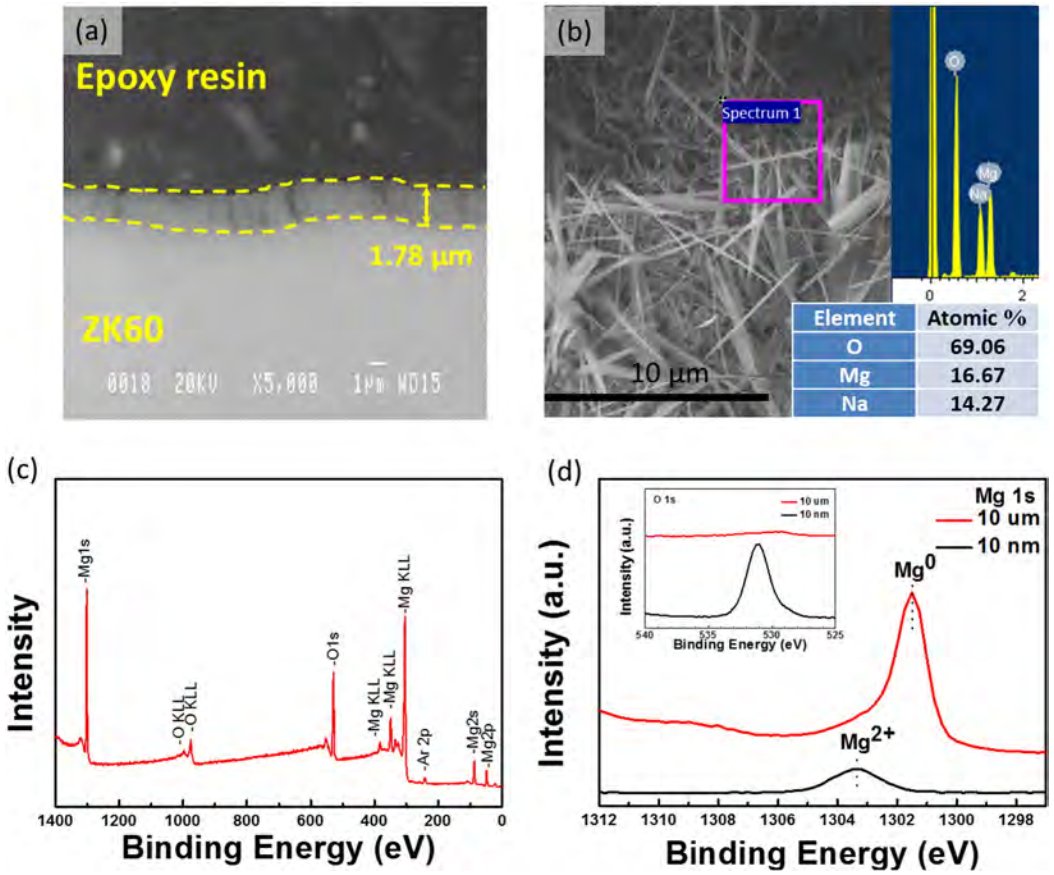

Fig. 3. (a) BSE cross-sectional image of 120 °C 24 h sample, (b) Surface morphology of the 120 °C 8 h sample together with the corresponding EDS spectrum and elemental composition, (c) XPS survey spectra of 120 °C 24 h sample, and (d) High-resolution XPS spectra of Mg and O of 120 °C 24 h sample.

solution commonly used in biological research and the constituents are (in mM) 137 NaCl, 2.7 KCl, 10 Na_2HPO_4, and 1.8 KH_2PO_4. Potentiodynamic polarization and electrochemical impedance spectroscopy (EIS) were carried out to evaluate the corrosion behavior of the samples before and after the treatment. A 5 mV sinusoidal perturbing signal in the frequency range between 100 kHz to 100 mHz was used during acquisition of the impedance spectra.

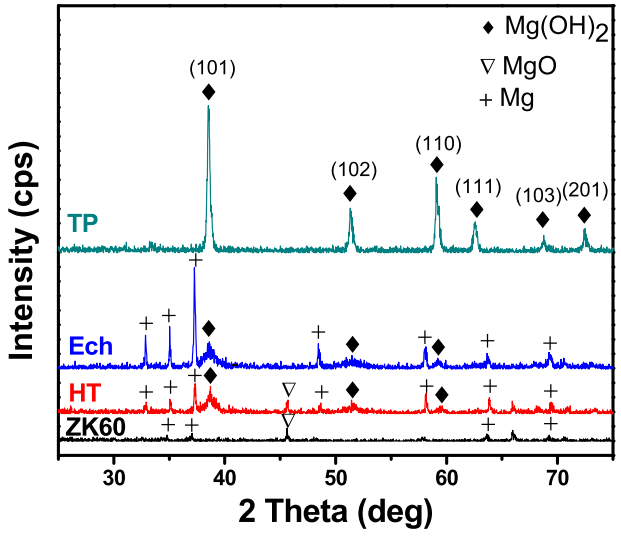

Fig. 4. XRD patterns: TP = treated product, Ech = sample after electrochemical tests, HT = sample after the hydrothermal experiment, and ZK60 = raw sample.

3. Results and discussion

Generation of $Mg(OH)_2$ by the alkaline hydrothermal method can be described by the following reactions:

$2H_2O\ (aq) + 2e- \rightarrow H_2\ (g) + 2OH^-\ (aq)$ (cathodic reaction)

$Mg\ (s) \rightarrow Mg^{2+}\ (aq) + 2e-$ (anodic reaction)

$Mg^{2+}\ (aq) + 2OH^-\ (aq) \rightarrow Mg(OH)_2\ (s)$ (product formation)

$Mg\ (s) + 2H_2O\ (aq) \rightarrow Mg(OH)_2\ (s) + H_2\ (g)$ (overall reaction).

In the hydrothermal method, the temperature and treatment time play key roles. In our experiments, the temperature is 60 °C and 120 °C and time is 1 h, 8 h, and 24 h in order to investigate the change in the morphology and corrosion properties of the $Mg(OH)_2$ films. The treated samples are designated as "treatment temperature treatment time" in the following description.

Fig. 1 shows the optical morphology of the ZK60 samples before and after the hydrothermal treatment. Before the HT treatment, the magnesium alloy ZK60 shows the typical metallic finish after mechanical polishing but after the HT reaction in the alkaline solution, the samples are uniformly coated with white films. The 60 °C sample exhibits a similar morphology and the film on the 120 °C sample is thicker.

The FE-SEM images of the samples prepared under different conditions are depicted in Fig. 2. The 60 °C samples show similar morphologies and the 60 °C 24 h sample is further analyzed (Fig. 2a) to study the formation of the $Mg(OH)_2$ film. The surface is covered by a film interspersed with flower-like crystals but crystallization on the surface is poor. Fig. 2b shows that when the temperature is raised to 120 °C for 1 h, the surface is almost fully covered by micrometer-size products decorated with clusters of long flakes. If the time is increased to 8 h, the surface shows a porous structure with small flakes and micrometer-size hexagonal holes. Many long strips about 500 nm wide and 10 μm long

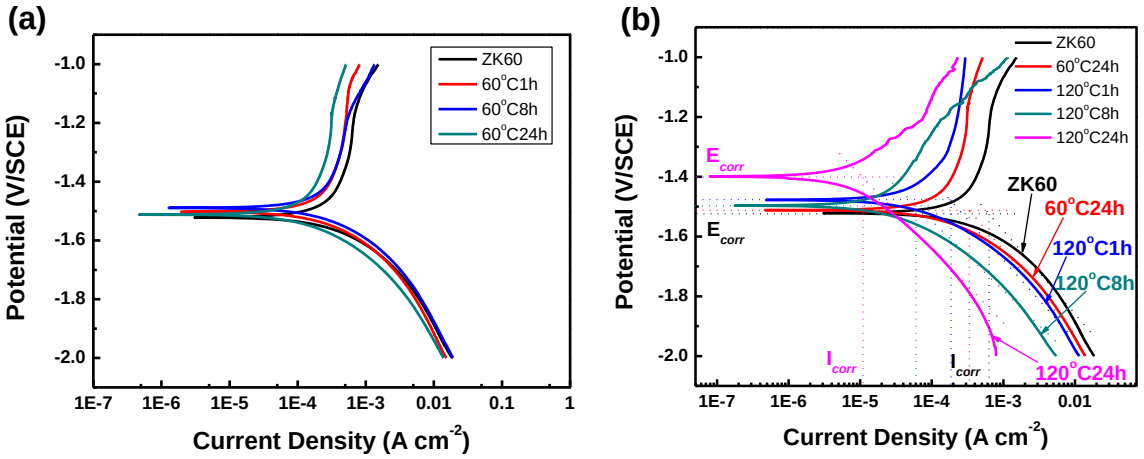

Fig. 5. Polarization curves acquired from the ZK60 samples in PBS before and after the hydrothermal treatment at different temperature and for different time.

are attached to the surface (Fig. 2c). Fig. 2d shows that if the time is further increased to 24 h, the hexagonal holes disappear and many micrometer-size hexagonal flakes are attached to the porous structure of small flakes. Hence, products with different morphologies are produced under different conditions. At a high temperature (120 °C), strips or hexagonal flakes are observed. Henrist et al. have reported that the hydrothermal conditions such as treatment time and temperature are key factors determining the product morphology, especially the shape and size [23]. Our experiments suggest that a high temperature accelerates nucleation and growth of $Mg(OH)_2$ and the treatment time affects the evolution of the surface morphology.

After treatment at 120 °C for 24 h, the sample is fully covered by the $Mg(OH)_2$ film. As shown in Fig. 3a, the $Mg(OH)_2$ film is quite uniform and the thickness is 1.78 ± 0.17 μm, which is the average of nine measurements conducted on three samples for statistical accountability. EDS shows the presence of O and Mg in the strip-like precipitates and a trace of Na from the residual solution. To determine the chemical composition, the XPS survey spectra of the 120 °C 24 h sample are shown in Fig. 3c which is dominated by the Mg 1s signal at 1301.6 eV as well as O 1s signal at 529.6 eV. The oxygen signal may originate from the HT treatment. The high-resolution XPS spectra in Fig. 3d are used to investigate the nature of the chemical bonding associated with transformation on the surface of HT treated sample. It shows the high-resolution XPS spectra of Mg 1s and O 1s. With sputtering, the Mg1s peak shifts from the oxidized state (Mg^{2+}) in the near surface to the metallic state (Mg^0) in the substrate. The O1s peak is found at the near surface and disappears in the substrate (inset picture), indicating that the main product in the near surface of the HT treated sample is magnesium hydroxide.

Fig. 4 displays the XRD patterns of the products before and after HT as well as after the electrochemical test. The XRD pattern of ZK60 reveals magnesium and magnesium oxide from the native oxide after exposing the polished sample to air. After the hydrothermal treatment, $Mg(OH)_2$ peaks appear indicating the formation of a hydroxide film. The $Mg(OH)_2$ film on the Ech sample does not delaminate after the electrochemical test and the sharp diffraction peaks from the treated product (TP) indicate good crystallinity. All the diffraction peaks can be indexed to the Brucite $Mg(OH)_2$ structure (PDF#76-0667) and the intensity of the diffraction peaks indicates the (101) preferred orientation. Lv et al. have found that the (101) plane belongs to the family of {011} plane, which is a stable one because Mg, O, and H atoms are closely packed on one plane [24]. The $Mg(OH)_2$ film with the (101) preferred orientation has a porous structure but offers protection to the substrate.

Potentiodynamic polarization is conducted in PBS at ambient temperature to determine the corrosion properties of the ZK60 samples before and after HT. Fig. 5a shows the polarization curves of the untreated ZK60 as well as samples after undergoing HT at 60 °C for 1 h, 8 h, and 24 h, respectively. Only the corrosion current density of the 60 °C 24 h sample increases slightly showing small improvement in the corrosion resistance. The other three curves exhibit similar trends and the corrosion current densities and corrosion potentials are nearly the same. The corrosion properties are enhanced significantly after HT at 60 °C. Fig. 5b shows that the curves of the HT samples shift up and left relative to the untreated ZK60 curve, indicating a more noble corrosion potential and smaller corrosion current density, respectively. Table 1 lists the corrosion current densities (I_{corr}) and corrosion potential (E_{corr}) obtained from the polarization curves by the Tafel extrapolation method. The corrosion potential of the 60 °C 24 h sample increases from −1.522 V to −1.512 V and the corrosion current density decreases from 6.325×10^{-4} A cm^{-2} to 3.346×10^{-4} A cm^{-2}. When the temperature is increased to 120 °C, the corrosion potentials of the 120 °C 1 h, 120 °C 8 h, and 120 °C 24 h samples are −1.478 V, −1.497 V, and −1.399 V and the corresponding corrosion current densities are 1.826×10^{-4} A cm^{-2}, 6.021×10^{-5} A cm^{-2}, and 1.083×10^{-5} A cm^{-2}, respectively. The 120 °C 8 h sample shows an I_{corr} with one order of magnitude reduction. Degradation of ZK60 is retarded after HT because of the barrier created by the $Mg(OH)_2$ film.

The corrosion mechanisms can sometimes be determined by analyzing the electrochemical impedance spectroscopy (EIS). The diameter of the capacitive semicircle of the Nyquist spectrum is closely related to the corrosion rate [25]. Fig. 6a shows that the diagrams are mainly composed of two depressive arcs at high and medium frequency ranges and

Table 1
I_{corr} and E_{corr} determined from the polarization curves.

Sample	ZK60	60 °C 24 h	120 °C 1 h	120 °C 8 h	120 °C 24 h
Potential (V/SCE)	−1.522	−1.512	−1.478	−1.497	−1.399
Current density (A cm^{-2})	6.325×10^{-4}	3.346×10^{-4}	1.826×10^{-4}	6.021×10^{-5}	1.083×10^{-5}

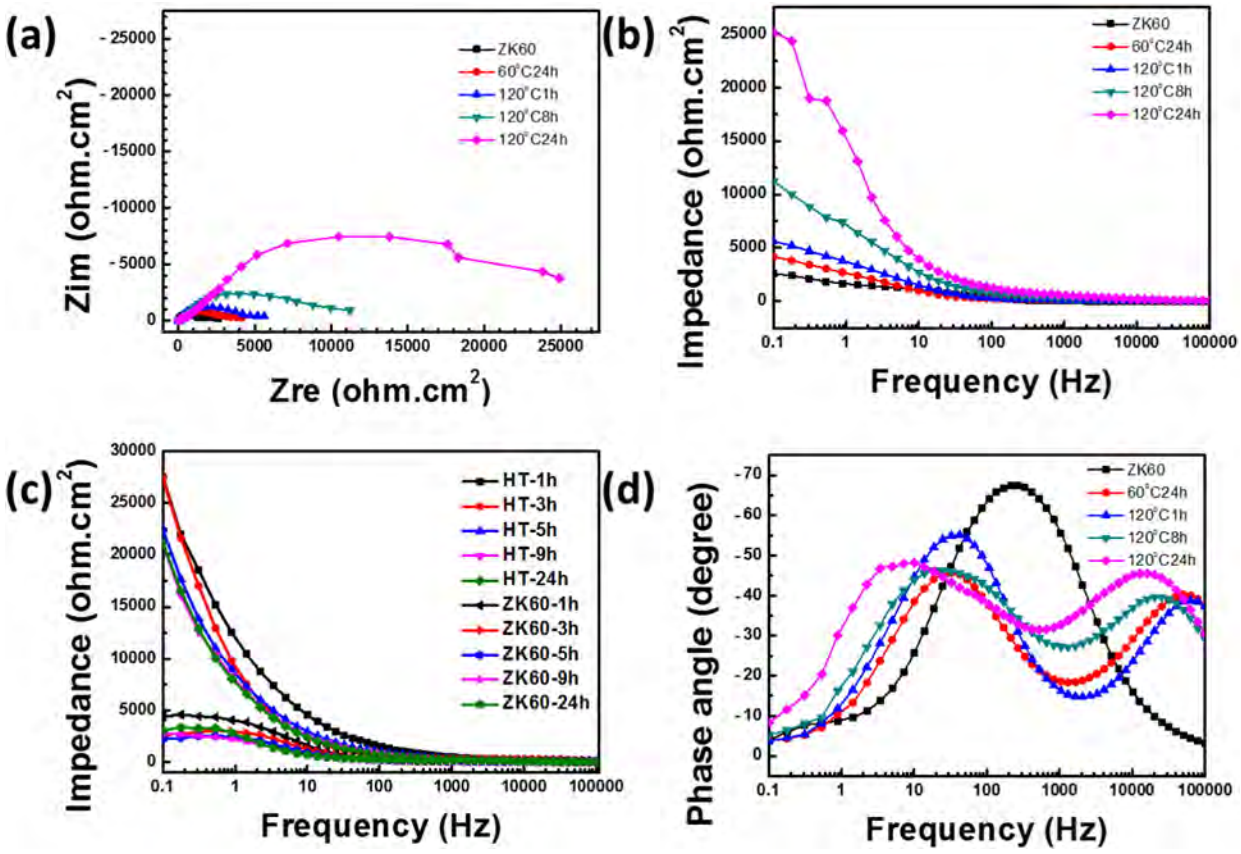

Fig. 6. Electrochemical impedance spectroscopy plots: (a) Nyquist plots, (b) Bode impedance plots, (c) Bode impedance plots measured at different time, and (d) Bode phase angle plots.

some scattered points in the low frequency region. The capacitive arcs are usually attributed to charge transfer, film effects, as well as mass transfer in the corrosion product layer [26]. After the HT treatment, the capacitive arcs are evidently enlarged, indicating that the corrosion rates on the treated samples are significantly reduced. Fig. 6b depicts the impedance of different samples. All the treated samples have larger impedance values than the untreated ZK60 sample and have the largest impedances at 0.1 Hz. The largest impedance of 2.5×10^5 Ω is obtained from the 120 °C 24 h sample. The bode impedance plots of ZK60 and HT treated sample at 120 °C 24 h measured at different time are displayed in Fig. 6c. After immersion for 1 h in PBS, the impedance of the HT sample is 27,531 Ω, while the impedance of untreated sample is 4389 Ω at 0.1 Hz. When the immersion time is increased, the impedances of the two samples both decrease. The impedances of the HT sample and ZK60 are stable at around 21,000 Ω and 3000 Ω, respectively, during immersion for 24 h. At the same time duration, the HT sample shows higher impedance than the untreated ZK60. The Bode phase angle plots of the samples before and after the HT treatment are displayed in Fig. 6d. Phase angle plots of the treated samples exhibit two peaks suggesting that the involvement of two time constants and the equivalent circuit in Fig. 7 illustrates the corrosion mechanism.

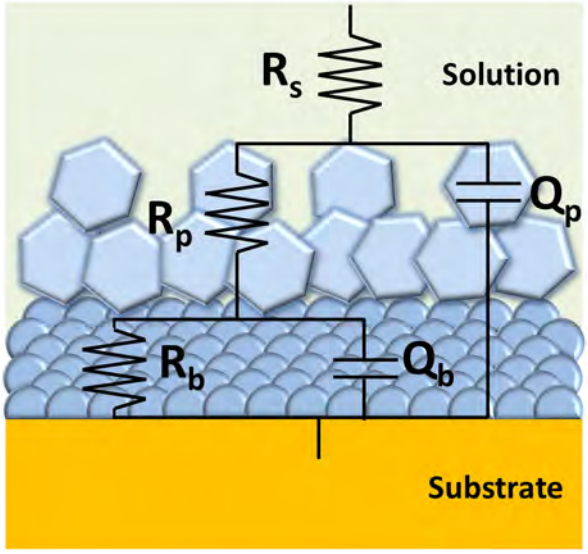

Fig. 7. Electrical equivalent circuit of the treated sample.

The impedance between the reference electrode (SCE) and working electrode (magnesium hydroxide film) consists of three parts: electrolyte, outer porous layer, and inner compact layer. The equivalent circuit consists of two constant phase angle elements (CPE) in series with the solution resistance (R_s). R_p is the outer porous layer resistance of the $Mg(OH)_2$ film in parallel with CPE Q_p and R_b is the inner compact layer resistance of the $Mg(OH)_2$ film in parallel with CPE Q_b. Owing to the dispersion effect caused by microscopic surface roughness, the capacitance of the film is replaced by CPE [27]. The impedance of the CPE is $Z_{CPE} = 1/Y_0(j\omega)^{-n}$ ($\Omega\ cm^2$), $0 < n < 1$, where ω is the angular frequency of AC voltage (rad s^{-1}) and Y_0 and n are frequency independent parameters. When $n = 1$, CPE shows pure capacitance and when $n = 0$, it represents pure resistance and inductance when $n = -1$ [28].

By using the equivalent circuit to fit the EIS spectra of the HT samples, the results of the corresponding fitted curves are displayed in Fig. 8 and the fitted data are shown in Table 2. The HT samples processed under different conditions show a similar EIS behavior in both the high-

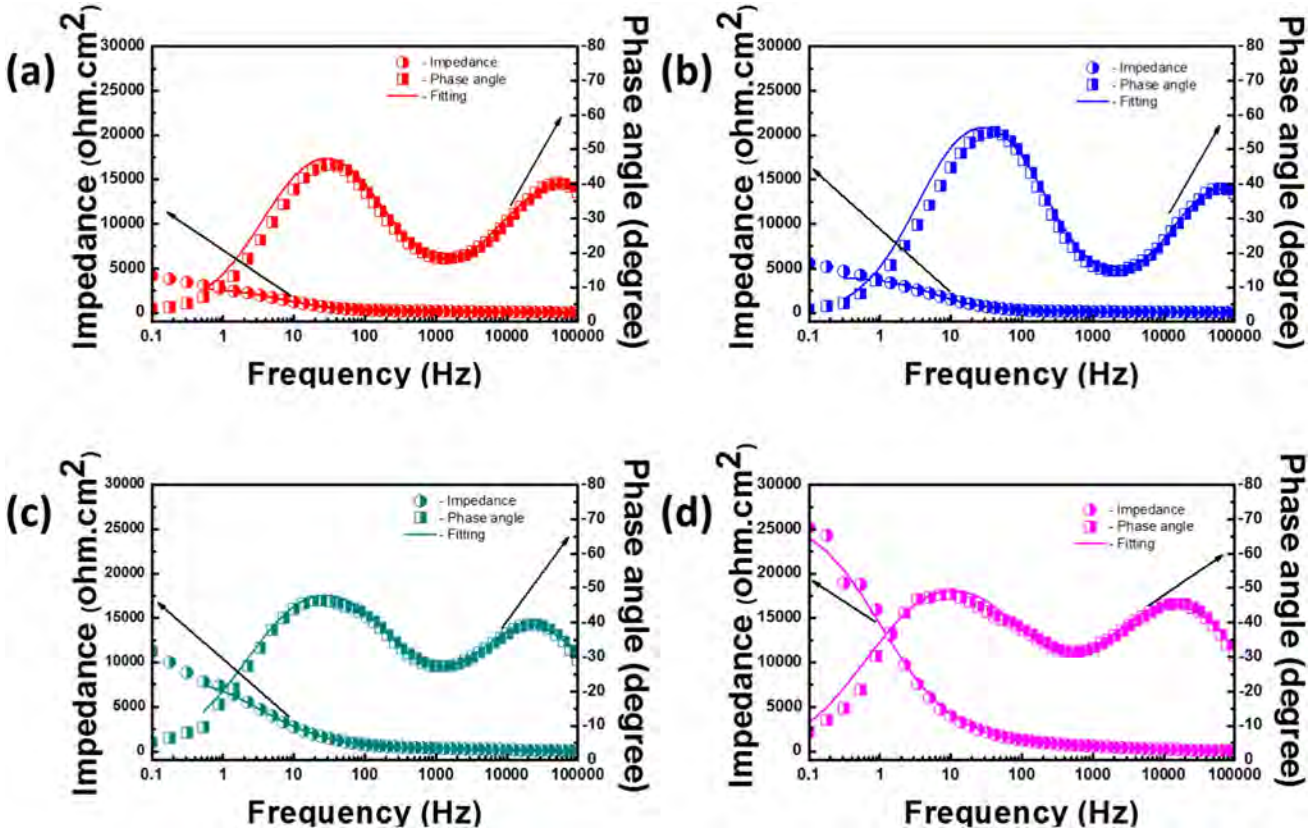

Fig. 8. Non-linear least square fits obtained for the EIS data of (a) 60 °C 24 h sample, (b) 120 °C 1 h sample, (c) 120 °C 8 h sample, and (d) 120 °C 24 h sample.

Table 2
Fitted results of EIS plots of the magnesium alloy ZK60 after the HT treatment under different conditions.

Sample	R_s (Ω cm^2)	Q_p (Ω^{-1} s^{-n} cm^{-2})	n_p	R_p (Ω cm^2)	Q_b (Ω^{-1} s^{-n} cm^{-2})	n_b	R_b (Ω cm^2)
60 °C 24 h	13.93	2.044×10^{-6}	0.7247	167.4	2.341×10^{-5}	0.8001	2542
120 °C 1 h	16.8	8.912×10^{-7}	0.7823	181.4	1.426×10^{-5}	0.8731	3100
120 °C 8 h	32.46	1.437×10^{-6}	0.7485	318.3	1.472×10^{-5}	0.7225	8407
120 °C 24 h	36.54	1.759×10^{-6}	0.7153	827.1	1.118×10^{-5}	0.7099	2.622×10^{4}

frequency and low-frequency ranges in the EIS plots. The high-frequency range reflects the outer $Mg(OH)_2$ porous layer, whereas the low-frequency range shows the inner compact layer properties [29,30]. The fitted results show that R_p and R_b of the 120 °C 24 h sample are larger than those of the other three samples. The polarization resistance ($R_p + R_b$) increases from 2.7×10^3 Ω cm^2 for the 60 °C 24 h sample to 2.7×10^5 Ω cm^2 for the 120 °C 24 h sample. The different corrosion resistance indicates different EIS behavior which is related to the different magnesium hydroxide structure. As the temperature and time are increased, the inner layer becomes more compact and dense and is able to offer better protection against electrolyte penetration into the substrate.

4. Conclusion

ZK60 magnesium alloy samples are treated by an alkaline hydrothermal method at different temperature and for different time. The morphology of the magnesium hydroxide changes from small flakes, strips, to hexagonal flakes depending on the hydrothermal conditions. The HT process at 60 °C only leads to slightly enhanced corrosion protection due to the partially covering $Mg(OH)_2$ films. A higher hydrothermal temperature accelerates the nucleation and growth rates of $Mg(OH)_2$ and the morphology $Mg(OH)_2$ changes with treatment time. The 120 °C 24 h sample with a 1.78 μm thick magnesium hydroxide film and preferred orientation of (101) shows the best corrosion resistance.

Acknowledgements

The work was financially supported by China Three Gorges University Talent Start-up Funds Nos. KJ2014B079 and KJ2014B080, Scientific Research Project of Yichang City No. A16-302-a14, as well as Hong Kong Research Grants Council (RGC) General Research Funds (GRF) No. CityU 11301215.

References

[1] J.X. Wang, L.T. Wang, Y.B. Fan, Adverse biological effect of TiO2 and hydroxyapatite nanoparticles used in bone repair and replacement, Int. J. Mol. Sci. 17 (2016).
[2] T.A. Grunewald, H. Rennhofer, B. Hesse, M. Burghammer, S.E. Stanzl-Tschegg, M. Cotte, J.F. Loffler, A.M. Weinberg, H.C. Lichtenegger, Magnesium from bioresorbable implants: distribution and impact on the nano- and mineral structure of bone, Biomaterials 76 (2016) 250–260.
[3] L.A. Meyer, Testing and Modeling Mechanical Properties of Ex Vivo Trabecular Bone, THE UNIVERSITY OF WISCONSIN, MADISON, 2016 275.
[4] S. Yao, Y.F. Li, Review on the development and application of magnesium alloys, Des. Manuf. Mechatronics Icdmm 2015 (2016) 1014–1020.
[5] M.P. Staiger, A.M. Pietak, J. Huadmai, G. Dias, Magnesium and its alloys as orthopedic biomaterials: a review, Biomaterials 27 (2006) 1728–1734.

[6] Y. Xin, T. Hu, P.K. Chu, In vitro studies of biomedical magnesium alloys in a simulated physiological environment: a review, Acta Biomater. 7 (2011) 1452–1459.
[7] R.C. Zeng, Y. Hu, F. Zhang, Y.D. Huang, Z.L. Wang, S.Q. Li, E.H. Han, Corrosion resistance of cerium-doped zinc calcium phosphate chemical conversion coatings on AZ31 magnesium alloy, Trans. Nonferrous Met. Soc. 26 (2016) 472–483.
[8] Q.L. Liu, X.D. Wang, X.K. Wang, X.W. Yan, X.J. Ma, Study of high emittance chemical conversion coatings for magnesium alloys, Surf. Eng. 30 (2014) 48–52.
[9] X.N. Gu, Y.F. Zheng, Y. Cheng, S.P. Zhong, T.F. Xi, In vitro corrosion and biocompatibility of binary magnesium alloys, Biomaterials 30 (2009) 484–498.
[10] R.Z. Xu, G.S. Wu, X.B. Yang, T. Hu, Q.Y. Lu, P.K. Chu, Controllable degradation of biomedical magnesium by chromium and oxygen dual ion implantation, Mater. Lett. 65 (2011) 2171–2173.
[11] G.S. Wu, K. Feng, A. Shanaghi, Y. Zhao, R.Z. Xu, G.Y. Yuan, P.K. Chu, Effects of surface alloying on electrochemical corrosion behavior of oxygen-plasma-modified biomedical magnesium alloy, Surf. Coat. Technol. 206 (2012) 3186–3195.
[12] Y. Yang, F. Scenini, M. Curioni, A study on magnesium corrosion by real-time imaging and electrochemical methods: relationship between local processes and hydrogen evolution, Electrochim. Acta 198 (2016) 174–184.
[13] Y. Wang, Z.Q. Huang, Q. Yan, C. Liu, P. Liu, Y. Zhang, C.H. Guo, G.R. Jiang, D.J. Shen, Corrosion behaviors and effects of corrosion products of plasma electrolytic oxidation coated AZ31 magnesium alloy under the salt spray corrosion test, Appl. Surf. Sci. 378 (2016) 435–442.
[14] H. Jeong, Y. Yoo, Synthesis and characterization of thin films on magnesium alloy using a hydrothermal method, Surf. Coat. Technol. 284 (2015) 26–30.
[15] Y.Y. Zhu, G.M. Wu, Y.H. Zhang, Q. Zhao, Growth and characterization of Mg(OH)(2) film on magnesium alloy AZ31, Appl. Surf. Sci. 257 (2011) 6129–6137.
[16] H.X. Zhang, Q. Li, L.Q. Li, J.C. Zhou, S.Y. Wang, F. Liu, P. Zhang, In vitro studies of hydrothermally treated magnesium alloy in common simulated body fluid, Trans. Inst. Met. Finish. 91 (2013) 141–148.
[17] X.M. Zhang, G.S. Wu, X. Peng, L.M. Li, H.Q. Feng, B.A. Gao, K.F. Huo, P.K. Chu, Mitigation of corrosion on magnesium alloy by predesigned surface corrosion, Sci. Rep. 5 (2015).
[18] J.F. Ou, W.H. Hu, M.S. Xue, F.J. Wang, W. Li, Superhydrophobic surfaces on light alloy substrates fabricated by a versatile process and their corrosion protection, ACS Appl. Mater. Interfaces 5 (2013) 3101–3107.
[19] T. Ishizaki, N. Kamiyam, E. Yamamoto, S. Kumagai, T. Sudare, N. Saito, Communication-in situ formation of anticorrosive Mg(OH)(2)/carbon composite film on magnesium alloy by ascorbic acid-assisted hydrothermal process, J. Electrochem. Soc. 162 (2015) C741–C743.
[20] Y.Y. Zhu, Q. Zhao, Y.H. Zhang, G.M. Wu, Hydrothermal synthesis of protective coating on magnesium alloy using de-ionized water, Surf. Coat. Technol. 206 (2012) 2961–2966.
[21] J. Feng, Y. Chen, X.H. Liu, T.D. Liu, L.Y. Zou, Y.T. Wang, Y.M. Ren, Z.J. Fan, Y.Z. Lv, M.L. Zhang, In-situ hydrothermal crystallization Mg(OH)(2) films on magnesium alloy AZ91 and their corrosion resistance properties, Mater. Chem. Phys. 143 (2013) 322–329.
[22] F.B. Gong, J. Shen, R.H. Gao, X. Xie, X. Luo, Enhanced corrosion resistance of magnesium alloy by a silane-based solution treatment after an in-situ formation of the Mg(OH)(2) layer, Appl. Surf. Sci. 365 (2016) 268–274.
[23] C. Henrist, J.P. Mathieu, C. Vogels, A. Rulmont, R. Cloots, Morphological study of magnesium hydroxide nanoparticles precipitated in dilute aqueous solution, J. Cryst. Growth 249 (2003) 321–330.
[24] J. Lv, L.Z. Qu, B.J. Qu, Controlled growth of three morphological structures of magnesium hydroxide nanoparticles by wet precipitation method, J. Cryst. Growth 267 (2004) 676–684.
[25] G.L. Song, A.L. Bowles, D.H. StJohn, Corrosion resistance of aged die cast magnesium alloy AZ91D, Mater. Sci. Eng. A 366 (2004) 74–86.
[26] Y.C. Xin, K.F. Huo, H. Tao, G.Y. Tang, P.K. Chu, Influence of aggressive ions on the degradation behavior of biomedical magnesium alloy in physiological environment, Acta Biomater. 4 (2008) 2008–2015.
[27] Y.L. Cheng, Z. Zhang, F.H. Cao, J.F. Li, J.Q. Zhang, J.M. Wang, C.N. Cao, A study of the corrosion of aluminum alloy 2024-T3 under thin electrolyte layers, Corros. Sci. 46 (2004) 1649–1667.
[28] H.L. Wu, Y.L. Cheng, L.L. Li, Z.H. Chen, H.M. Wang, Z. Zhang, The anodization of ZK60 magnesium alloy in alkaline solution containing silicate and the corrosion properties of the anodized films, Appl. Surf. Sci. 253 (2007) 9387–9394.
[29] S.C. Chung, J.R. Cheng, S.D. Chiou, H.C. Shih, EIS behavior of anodized zinc in chloride environments, Corros. Sci. 42 (2000) 1249–1268.
[30] P.B. Su, X.H. Wu, Z.H. Jiang, Y. Guo, Effects of working frequency on the structure and corrosion resistance of plasma electrolytic oxidation coatings formed on a ZK60 Mg alloy, Int. J. Appl. Ceram. Technol. 8 (2011) 112–119.